*Int. J. Heat Mass Transfer.* Vol. 36, No. 1, pp. 89–100, 1993
Printed in Great Britain

0017-9310/93 $5.00 + 0.00


# On the stability of the near shore waters of a lake when subject to solar heating

D. E. FARROW and J. C. PATTERSON
Centre for Water Research, University of Western Australia, Australia

(*Received* 8 *August* 1991)

**Abstract**—During the day, water in a lake or reservoir absorbs solar radiation according to Beer's law. As the depth decreases towards the shore, more of the radiation penetrates to the bottom, leading to a region of warmer water attached to the lower boundary which is a potentially unstable temperature profile. This situation is modelled by a fluid contained in a triangular domain with a horizontal upper surface. The fluid is subject to internal heating associated with Beer's law and a bottom boundary heat flux associated with the radiation that is not absorbed by the water column. Previous work suggests that the preferred mode for the instability consists of longitudinal rolls with their axes aligned with the slope. As the bottom slope becomes small, the stability problem becomes independent of the base flow and the originally three-dimensional (3-D) problem is reduced to a two-dimensional (2-D) problem between horizontal and parallel plates. A quasi-static, linear stability analysis suggests that, for geophysical parameters, the model is locally unstable in a region centred away from the shore.

## 1. INTRODUCTION

THE FLOODING of a lake or reservoir basin usually involves the inundation of many small valleys around its perimeter. These flooded valleys (which are then called sidearms) are typically only a few metres deep where they join with the main body of the reservoir. Sidearms are often well protected from the wind and so thermal forcing associated with differential heating and cooling is an important mechanism for promoting exchange between the sidearm and the main body of the reservoir. In a recent paper, Farrow and Patterson [1] developed a model for the daytime circulation in a lake or reservoir sidearm, based on the natural convection of a fluid contained in a two-dimensional (2-D) triangular domain with a horizontal upper surface. The flow was driven by the buoyancy induced by two heating mechanisms. First, an internal heating term given by $Q = Q_0 \exp(\eta z')$ °C s$^{-1}$ where $\eta$ is the attenuation coefficient and $z'$ is measured positive upwards from the upper surface was included in the temperature equation. This internal heating term is formulated from Beer's law for the absorption of solar radiation (see, for example, Rabl and Nielson [2]). Second, a boundary heat flux was applied at the sloping bottom, the strength of which depended on the amount of radiation penetrating the entire local depth. Thus, in the shallow regions, the depth averaged volumetric heating rate is greater than in the deeper regions, leading to a surface flow out from the shallow, near shore regions to the deeper parts. Field measurements [3] have indicated that this mechanism, and the corresponding reverse circulation generated at night by surface cooling, may be responsible for significant transport of suspended or dissolved material from the near shore regions of lakes to the central parts.

In ref. [1], asymptotic solutions for the 2-D ($v' \equiv 0$, $\partial/\partial y' \equiv 0$) temperature and flow fields were found as the bottom slope of the model sidearm shown in Fig. 1 became small. As will be seen below, these solutions showed that the temperature structure could be divided into two regions. Near the shore ($x' = 0$), most of the radiation reaches the bottom and this, combined with vertical conduction and the topography, leads to nearly vertical isotherms with a potentially unstable temperature gradient near the bottom boundary. The source of the potential instability is the heat flux boundary condition applied at the bottom boundary. Further out in the deeper regions, very little of the radiation reaches the bottom and most is absorbed in a relatively shallow layer near the surface and so in this region the isotherms are horizontal. These results are consistent with available field observations of reservoir sidearms. The aim of this paper is to examine the stability of the asymptotic solutions of ref. [1] and to determine a Grashof number below which secondary motion will not occur.

The stability problem discussed in this paper falls into a large class of Bénard type stability problems and includes the effects of sloping and non-parallel boundaries, non-monotonic temperature profiles and fixed flux rather than fixed temperature boundary conditions and the results therefore have a much wider applicability than the particular problem discussed here. In the present case, the source of the instability is a heat flux applied along a nearly horizontal boundary. The results for heated inclined plates in an infinite fluid [4, 6] and inclined, differentially heated rectangular cavities [7, 9] suggest that when the boundary that is the source of the instability is nearly horizontal then the least stable mode consists of longitudinal vortices with their axes aligned with the slope, as shown in Fig. 1. This is in contrast to the wave insta-

## NOMENCLATURE

$A$ bottom slope
$\mathbf{A}, \mathbf{B}, \mathbf{D}_j, \mathbf{E}_j, \mathbf{K}, \mathbf{K}^*, \mathbf{P}_j, \mathbf{R}$ matrices for numerical method
$C_p$ specific heat of water
$g$ acceleration due to gravity
$Gr$ Grashof number, $g\alpha I_0/(\rho_0 C_p \kappa^3 \eta^4)$
$Gr_c$ critical Grashof number
$Gr_c^*$ minimum over $x$ of $Gr_c$
$Gr_{\min}$ minimum Grashof number
i $\sqrt{-1}$
$\mathbf{I}$ identity matrix
$I_0$ intensity of radiation incident on the surface
$J$ number of grid points
$k$ wave number
$k_c$ critical wave number
$p'$ pressure
$p$ non-dimensional pressure, $p'g\alpha I_0/(C_p \kappa \eta^2)$
$P$ perturbation pressure
Re $\{z\}$ real part of complex number $z$
$s$ growth rate of perturbation
$t$ non-dimensional time, $t'\kappa\eta^2$
$t'$ time
$T$ non-dimensional temperature, $(T'-T_0)\rho_0 C_p \kappa\eta/I_0$
$T'$ temperature
$T_0$ reference temperature
$U$ vector for numerical method
$u, v, w$ non-dimensional velocities: $u = u'/(A\,Gr\,\kappa\eta)$, $v = v'/(A\,Gr\,\kappa\eta)$ and $w = w'/(A^2\,Gr\,\kappa\eta)$
$u', v', w'$ velocities
$V, W$ perturbation velocities
$x, y, z$ non-dimensional coordinate system: $x = A\eta x'$, $y = \eta y'$ and $z = \eta z'$
$x', y', z'$ Cartesian coordinate system, $z$ vertical
$\Delta z$ discretization step, $1/J$.

Greek symbols
$\alpha$ thermal expansion coefficient
$\delta$ thermal boundary layer thickness
$\varepsilon$ perturbation parameter
$\eta$ attenuation coefficient
$\theta, \Theta$ perturbation temperature
$\kappa$ thermal diffusivity
$\nu$ kinematic viscosity
$\pi_j$ matrix for numerical method
$\rho_0$ reference density
$\sigma$ Prandtl number, $\nu/\kappa$
$\psi$ perturbation stream function
$\Psi$ vector for numerical method.

Subscripts
0 $k_c = 0$ solution
$x$ partial differentiation.

bility which consists of amplifying waves travelling up the slope. In the current work, longitudinal vortices are the assumed form of the instability.

An important aspect of the stability problem under consideration in this paper is that the base temperature solution is not monotonic. This is because the internal heating term formulated from Beer's law leads to stable temperature gradients while the bottom boundary heating leads to unstable gradients. This means that the model sidearm does not necessarily become unstable over the entire local depth. A problem of this kind was studied by Matthews [10] where the background temperature structure was cubic, leading to a stable–unstable–stable density structure. Matthews found that a convective cell was set up in the central unstable region with a counter rotating cell in each of the stable regions driven by momentum transferred from the central region via viscosity. A similar problem was discussed by Roberts [11], who considered water at close to its density minimum. Thus, even though the temperature profile was linear, the density profile was not with stable fluid overlying unstable fluid. In that paper, the most important effect of the stable layer was to isolate the unstable layer from the surface boundary condition which leads to a radical change in the critical wave number. A similar behaviour appears in the current case as will be seen later.

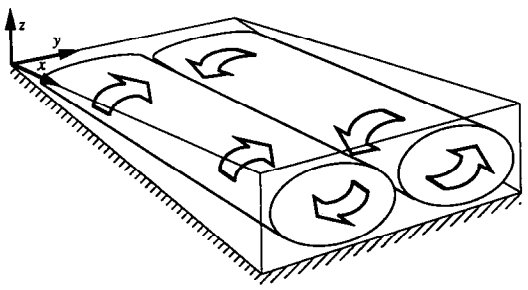


FIG. 1. Schematic of the geometry of the flow domain and the assumed form of the 3-D instability.

In Section 2 of this paper, the linear stability equations are established for the day time model considered in ref. [1]. The resulting equations, though linear, are not amenable to direct analysis. However, the nature of the temperature boundary conditions allows some assumptions to be made that simplify the analysis, at least for part of the problem, and this is done in Section 3. The results of Section 3 are not conclusive and so in Section 4 the full stability equations are solved numerically. The analytical and numerical results are discussed in Section 5.

## 2. PROBLEM FORMULATION

For the problem under consideration in this paper, the non-dimensional Navier–Stokes equations in three dimensions are

$$u_t + A^2\,Gr(uu_x + A^{-2}vu_y + wu_z) = -p_x + \sigma(A^2u_{xx} + u_{yy} + u_{zz}) \quad (1)$$

$$v_t + A^2\,Gr(uv_x + A^{-2}vv_y + wv_z) = -p_y + \sigma(A^2v_{xx} + v_{yy} + v_{zz}) \quad (2)$$

$$A^2w_t + A^4\,Gr(vw_x + A^{-2}vw_y + ww_z) = -p_z + \sigma A^2(A^2w_{xx} + w_{yy} + w_{zz}) + T \quad (3)$$

$$T_t + A^2\,Gr(uT_x + A^{-2}vT_y + wT_z) = A^2T_{xx} + T_{yy} + T_{zz} + e^z \quad (4)$$

$$A^2u_x + v_y + A^2w_z = 0 \quad (5)$$

with boundary conditions

$$u = v = w = 0 \quad \text{on} \quad z = -x \quad (6)$$

$$u_z = v_z = w = 0 \quad \text{on} \quad z = 0 \quad (7)$$

$$T_z = 0 \quad \text{on} \quad z = 0 \quad (8)$$

$$T_n = -e^{-x} \quad \text{on} \quad z = -x \quad (9)$$

and the initial conditions $u = v = w = T = 0$ at $t = 0$ and $z = -x$ is the bottom boundary and $z = 0$ is the free surface. The non-dimensionalization scheme is summarized in the Nomenclature. These scales are obtained by using the vertical length scale $\eta^{-1}$ and the time scale $(\kappa\eta^2)^{-1}$ and assuming that the most important terms are buoyancy, pressure, vertical shear and inertia. A more detailed discussion of the non-dimensionalization scheme is given in ref. [1]. The $e^z$ term on the right-hand side of equation (4) represents the internal heating due to the absorption of solar radiation. The heat flux bottom boundary condition (9) is derived by assuming that the energy that is not absorbed by the water column is absorbed by the bottom and then re-emitted as a boundary heat flux.

In ref. [1], at 2-D asymptotic solution for equations (1)–(9) was found as $A \to 0$. Mathematically, this is equivalent to taking the lowest order in $A$, setting $v = 0$ and neglecting variations in the $y$ direction in equations (1)–(9). In what follows, this asymptotic solution is denoted by $T^{(0)}$, $u^{(0)}$, $w^{(0)}$ and $p^{(0)}$ where each of these functions is independent of $y$ and, as will be seen later, only $T^{(0)}$ is required in the present analysis. For the purposes of this paper, it is assumed that the $O(A^0)$ solution is quasi-static; that is, the evolution of the $O(A^0)$ solution does not affect its instantaneous stability. The significance of this kind of assumption has been considered by a number of authors [12–14] who found that the assumption was not valid for a step change in the temperature, in which case the critical $Gr$ was severely underestimated. In the present case, the fixed flux boundary conditions ensure that there are no step changes in the temperature structure.

The $O(A^0)$ solution is now perturbed according to the expressions

$$\begin{aligned} u &= u^{(0)} \\ v &= \varepsilon V \\ w &= w^{(0)} + \frac{\varepsilon}{A^2}W \\ T &= T^{(0)} + \varepsilon\Theta \\ p &= p^{(0)} + \varepsilon P \end{aligned} \quad (10)$$

where $\varepsilon \ll 1$ is the perturbation parameter. The $\varepsilon/A^2$ factor of the $w$ perturbation ensures that the perturbation velocities $V$ and $W$ in the $(y, z)$ plane scale in the same way. There is no perturbation to the $x$ component of the velocity since the assumed form of the instability consists of longitudinal vortices as shown in Fig. 1. Substituting the perturbed solutions (10) into equations (1)–(5) and linearizing with respect to $\varepsilon$ and $A$ yields a system of equations for the perturbing quantities

$$Gr\,Wu_z^{(0)} = -P_x \quad (11)$$

$$V_t = -P_y + \sigma(V_{yy} + V_{zz}) \quad (12)$$

$$W_t = -P_z + \sigma(W_{yy} + W_{zz}) + \Theta \quad (13)$$

$$\Theta_t + Gr\,WT_z^{(0)} = \Theta_{yy} + \Theta_{zz} \quad (14)$$

$$V_y + W_z = 0. \quad (15)$$

Note that the only place that the $O(A^0)$ velocity enters the equations is via the $x$-momentum equation (11) and only $u^{(0)}$ and $T^{(0)}$ are involved in equations (11)–(15). By eliminating the pressure perturbation $P$ from equations (12) and (13), the stability equations can be made independent of the zero order velocity. This is not surprising since, as $A \to 0$, the dimensional velocities vanish. In fact, it was shown in ref. [1] that the dimensional horizontal velocity was $O(A)$, hence, if the velocity were to have an effect on the stability problem, $A$ must appear as a parameter of the stability problem. Since $A$ has been explicitly excluded from the stability equations by linearizing with respect to $A$, it follows that the stability is independent of $u^{(0)}$ and only a knowledge of $T^{(0)}$ is required. The boundary value problem for $T^{(0)}$ is

$$T_t^{(0)} = T_{zz}^{(0)} + e^z \quad (16)$$

$$T^{(0)} = 0 \quad \text{at} \quad t = 0. \quad (17)$$

$$T_z^{(0)} = 0 \quad \text{on} \quad z = 0 \quad (18)$$

$$T_z^{(0)} = -e^{-x} \quad \text{on} \quad z = -x \quad (19)$$

which is a standard unsteady, one-dimensional (1-D) heat conduction problem, the solution of which is [1]

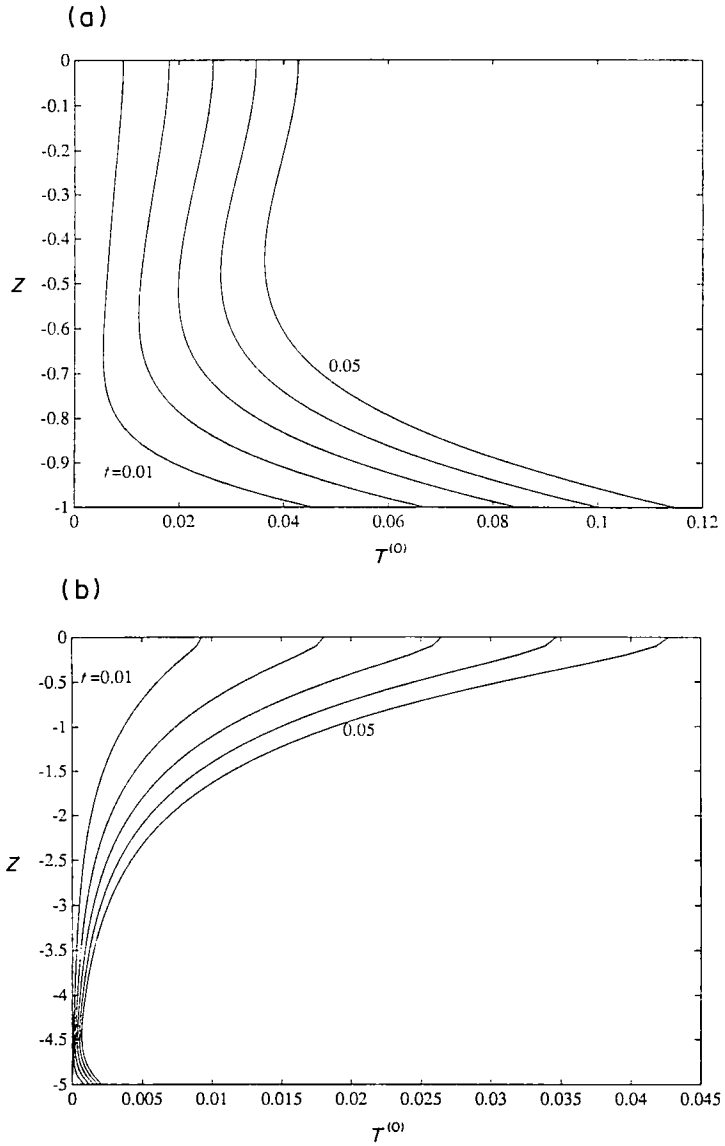


FIG. 2. Temperature profiles (equation (20)) for various times at: (a) $x = 1$; (b) $x = 5$.

$$T^{(0)} = \frac{t}{x} - e^{-z} + \frac{z^2}{2x} + z + \tfrac{1}{3}x + \frac{1}{x}(1 - e^{-x}) - \frac{2}{x}\sum_{n=1}^{\infty}\left[\frac{1}{(n\pi/x)^2} - \frac{1-(-1)^n e^{-x}}{1+(n\pi/x)^2}\right] \times \exp\left(-\left(\frac{n\pi}{x}\right)^2 t\right)\cos\left(\frac{n\pi}{x}z\right). \quad (20)$$

Figure 2 shows a series of temperature profiles at different times at two different $x$ locations from equation (20). In Fig. 2(a), most of the radiation penetrates to the bottom, leading to an increase in temperature with depth near the bottom. In Fig. 2(b), the local depth is greater meaning that most of the heat is absorbed internally, leading to stable temperature gradients near the surface. Note that $T^{(0)}$ does not reach steady state since heat is continuously being added and none is allowed to escape either through the boundaries or horizontally. A quasi-steady state is achieved when the transient terms in equation (20) have died away after which time the temperature profile is unchanged except for an increase in the vertically averaged temperature. Figure 3 shows isotherms in

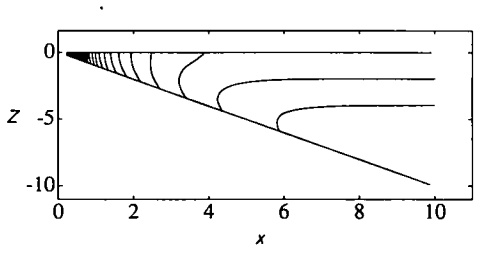


FIG. 3. Temperature contours at $t = 1.0$ showing the nearly vertical isotherms near the tip and the largely horizontal isotherms further out from the tip. The contour interval is 1.0.

the model sidearm at $t = 1$. For $x < 2$, the isotherms are nearly vertical while for $x > 5$, they are close to horizontal since most of the radiation is absorbed near the surface and the bottom boundary plays a less important role in determining the temperature structure.

Eliminating the pressure from equations (12) and (13) and introducing a stream function $\psi$ where $V = -\psi_z$ and $W = \psi_y$ yields

$$\nabla^2\psi_t = \sigma\nabla^4\psi + \Theta_y$$
$$\Theta_t + Gr\,\psi_y T_z^{(0)} = \nabla^2\Theta \tag{21}$$

where $\nabla^2 = \partial^2/\partial y^2 + \partial^2/\partial z^2$. The $x$-momentum equation (11) is no longer part of the stability problem under consideration in this paper. Thus, the initial 3-D stability problem has been reduced to a 2-D problem in the infinite strip $-x < z < 0$ in the $(y, z)$ plane. The boundary conditions are

$$\Theta_z = 0 \quad \text{on} \quad z = -x, 0$$
$$\psi = \psi_{zz} = 0 \quad \text{on} \quad z = 0$$
$$\psi = \psi_z = 0 \quad \text{on} \quad z = -x. \tag{22}$$

The above scaling has the physical interpretation that any instability will be a local phenomenon. This has the consequence that $x$ is now only a parameter of the stability problem and serves to specify what the local conditions are.

The small disturbances are now assumed to have the particular form

$$\Theta = \text{Re}\,\{\theta(z)\,e^{st+iky}\}$$
$$\psi = \text{Re}\,\{ik\psi(z)\,e^{st+iky}\}. \tag{23}$$

Here, $k$ is the (real) wave number of the disturbance, $s$ the instantaneous growth (or decay) rate. Substituting these expressions into the stability equations (21) gives

$$(D^2 - k^2 - s)\theta = -Gr\,k^2\psi DT^{(0)} \tag{24}$$
$$(D^2 - k^2)(D^2 - k^2 - s/\sigma)\psi = -\theta \tag{25}$$

where $D \equiv \partial/\partial z$ and $\theta$ and $\psi$ are functions of $z$ only. Interest here lies in under what condition is the system marginally stable, that is when $s = 0$. Substituting $s = 0$ into the above equations yields the marginal stability equations

$$(D^2 - k^2)\theta = -Gr(k; x, t)k^2\psi DT^{(0)}$$
$$(D^2 - k^2)^2\psi = -\theta \tag{26}$$

with the boundary conditions

$$\theta_z = 0 \quad \text{on} \quad z = 0, -x$$
$$\psi = \psi_{zz} = 0 \quad \text{on} \quad z = 0$$
$$\psi = \psi_z = 0 \quad \text{on} \quad z = -x. \tag{27}$$

These two equations and their associated boundary conditions represent an eigenvalue problem for $Gr(k; x, t)$ where, as suggested by the notation, the eigenvalue is a function of the parameters $k$, $x$ and $t$. Because the equations and boundary conditions are homogeneous there will only be certain values of $Gr$ that will allow a non-trivial solution. The $Gr$ that is of most interest here is the minimum over $k$ of the smallest positive $Gr$ at each value of $k$ since only positive values of $Gr$ are physically realisable. The task, then, is to calculate the critical Grashof number $Gr_c$ where $Gr_c$ is given by

$$Gr_c(x, t) = \min_{k \geq 0} Gr_{\min}(k; x, t) \tag{28}$$

where $Gr_{\min}(k; x, t)$ denotes the smallest positive $Gr$ at a particular value of $k$, $x$ and $t$. The critical Grashof number $Gr_c$ is a function of $x$ and $t$. The aim of this paper is to arrive at a lower bound on $Gr$ below which secondary motion will not occur and this therefore corresponds to the minimum over $x$ of $Gr_c$ and is denoted by $Gr_c^*$.

## 3. ANALYTIC SOLUTION

Unfortunately, the stability equations (26) include the term $-Gr\,k^2\psi DT^{(0)}$ which makes solution of the equations difficult to find for a general $DT^{(0)}$. However, Chapman and Proctor [15] have shown that if $DT^{(0)}$ is constant and the upper and lower boundary conditions on $\theta$ are that the flux vanishes then the critical wave number at which $Gr_{\min}$ occurs is $k = 0$. In fact, they show that the zero critical wave number holds for both linear and non-linear instabilities. Even though in the current case $DT^{(0)}$ is not constant, this property of the stability problem can be exploited to find an expression for the critical Grashof number analytically for at least part of the parameter range.

Following Roberts [11], $\psi$, $\theta$ and $Gr_c$ are expanded in the following way for $k \ll 1$:

$$Gr_c = Gr_{c0} + k^2\,Gr_{c2} + \cdots$$
$$\theta = \theta_0 + k^2\theta_2 + \cdots$$
$$\psi = \psi_0 + k^2\psi_2 + \cdots. \tag{29}$$

The marginal stability equations (26) only include even powers of $k$ and so only even powers of $k$ are included in the above expansions. Substituting these expansions into equations (26) and equating like powers of $k$ yields a sequence of linear equations that can be solved recursively. The $O(k^0)$ equations are

$$D^2\theta_0 = 0$$
$$D^4\psi_0 = -\theta_0 \tag{30}$$

which have the simple solutions (after using the boundary conditions)

$$\theta_0 = 1$$
$$\psi_0 = -\tfrac{1}{48}z(z + x)^2(2z - x). \tag{31}$$

Note that $\psi_0$ given above consists of a convective cell that occupies the entire local depth. The value of $Gr_{c0}$ can be obtained by a solvability condition at the next order. The $O(k^2)$ temperature perturbation equation is

$$D^2\theta_2 = \theta_0 - Gr_{c0}\,\psi_0 DT^{(0)}. \quad (32)$$

Integrating the above equation with respect to $z$ over the local depth and using the no flux boundary conditions yields

$$0 = \int_{-x}^{0} \theta_0\,dz - Gr_{c0}\int_{-x}^{0} \psi_0 DT^{(0)}\,dz \quad (33)$$

which can be written as (after substituting for $\theta_0$ and $\psi_0$)

$$Gr_{c0} = \frac{-48x}{\int_{-x}^{0} z(z+x)^2(2z-x)DT^{(0)}\,dz}. \quad (34)$$

Substituting for $DT^{(0)}$ into the above equation yields an expression for $Gr_{c0}$ which is a function of $x$ and $t$

$$Gr_{c0} = 576x\Bigg[576(1-e^{-x}) - 72x(3+5e^{-x}) + 12x^3 - 72x^2 e^{-x} - x^5 + \frac{144}{x} \times \sum_{n=1}^{\infty}\left[\left(\frac{x}{n\pi}\right)^2 - \frac{1-(-1)^n e^{-x}}{1+(n\pi/x)^2}\right]\left(\frac{x}{n\pi}\right)^4 \times (-1)^n(8-(n\pi)^2)\,e^{-(n\pi/x)^2 t}\Bigg]^{-1}. \quad (35)$$

Figure 4 shows a series of curves of $Gr_{c0}$ for various times. Note that even though $T^{(0)}$ does not have a steady state since the average temperature increases without limit with time, as discussed previously, $DT^{(0)}$ does reach a steady value and the time at which that occurs depends on $x$. The time for $DT^{(0)}$ to reach a steady value increases with $x$ and is associated with the time taken for heat to diffuse across the local depth. This fact manifests itself in Fig. 4 via the convergence of all the curves as $x \to 0$. Another property of the curves in Fig. 4 is the singular behaviour of $Gr_{c0}$ as $x \to 0$. The reason for this is that $DT^{(0)}$ is bounded as $x \to 0$ but viscosity will increase in importance as the local depth vanishes and thus the model is unconditionally stable as $x \to 0$.

For a fixed $t$, $Gr_{c0}$ given by equation (35) is singular at a particular $x$ which corresponds to the denominator in equations (35) vanishing. At $t = 0.005$, $Gr_{c0}$ is singular at $x \approx 1$ and at $t = \infty$, $Gr_{c0}$ is singular at $x \approx 1.4$. For values of $x$ greater than the singular value, $Gr_{c0}$ is negative and the resulting curves do not appear in Fig. 4. The singular behaviour and the associated negative values for $Gr_{c0}$ arise because there is a shift in the nature of the overall temperature structure as $x$ becomes close to the singular value. The shift occurs as the main component of the heating changes from the bottom boundary heating for small $x$ to the internal $e^-$ heating for large $x$. The $e^-$ heating is stabilizing and so the negative $Gr_{c0}$ has the physical interpretation that if the fluid is to become unstable over the entire water column, gravity must change sign. A similar behaviour was noted by Roberts [11]. Roberts considered water at close to its density minimum and thus even though the background temperature structure was linear, the density was not with stable fluid overlying an unstable region. Roberts found a similar departure from the $k_e = 0$ property when the stably stratified region dominated the density structure.

Despite the stably stratified surface region at large $x$, there is still a region near the bottom boundary where the temperature is increasing with depth since there is a heat flux boundary condition at $z = -x$. This can be seen in Fig. 2(b). Clearly this region would become unstable if the temperature gradients were sufficiently large and yet the results of the present analysis suggests that these profiles are unconditionally stable. This inconsistency can be attributed

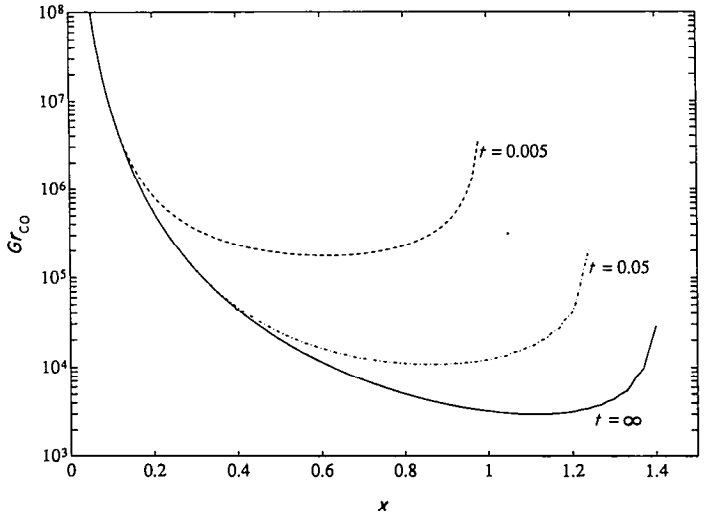


FIG. 4. Graphs of $Gr_{c0}$ (equation (35)) at various times as a function of $x$.

directly to the zero critical wave number assumption used in the above analysis. The zero critical wave number assumption is based on the fixed flux boundary conditions applied at $z = 0$ and $-x$. However, as $x$ increases the unstable region near the bottom is isolated from the $z = 0$ boundary by a stably stratified surface region. Hence, the zero critical wave number assumption will not necessarily hold for large $x$ since the boundary condition felt by the unstable region is not necessarily insulated. The effect of a non-zero critical wave number is addressed in the next section where the stability equations (26) are solved numerically with no assumptions about the critical wave number.

As shown in Fig. 4, the values of $Gr_{c0}$ decrease with increasing $t$, indicating that the model becomes less stable with time, but approaching the values indicated by the $t = \infty$ result. This is to be expected for the following reasons. The vertical temperature structure arises via two mechanisms: internal heating and a boundary heat flux. Only the heat flux boundary condition at $z = -x$ gives rise to unstable temperature gradients. This means that the unstable temperature gradient must be a maximum at $z = -x$; there are no mechanisms available to give rise to greater unstable temperature structures within the fluid. The unstable region is restricted to the conductive boundary layer near $z = -x$ and the temperature gradient across that layer is nearly constant with time since it is fixed at $z = -x$. Thus, as time increases and the boundary layer thickness increases, the same temperature gradient is applied over a greater depth. This process increases the local Grashof number based on the boundary layer thickness which in turn leads to the temperature profile becoming less stable as time increases.

The aim of this paper is to calculate a critical Grashof number below which secondary motion will not occur. For a particular time and assuming that the critical wave number is zero, this will be the minimum over $x$ of $Gr_{c0}$. Assuming that the heating phase has been underway for 12 h, $\eta = 2\ \mathrm{m}^{-1}$ and molecular values for $\kappa$ (and so 12 h corresponds to a non-dimensional time of $t = 0.025$) yield a tentative value for the critical Grashof number below which secondary motion will not occur of $Gr_c^* = 4.2 \times 10^4$. This value is tentative since it is not clear from the analysis of this section when the zero critical wave number assumption breaks down and whether the breakdown will affect the value of $Gr_c^*$. The numerical results of the next section will show that the breakdown does not effect the value of $Gr_c^*$. Also, $Gr_c^* = 4.2 \times 10^4$ is likely to be an underestimation of the true critical Grashof number due to effects that are not included in the model under consideration in this paper. These include the effects of sidewalls in the $y$-direction that would, via boundary conditions, put a lower limit on the critical wave number. If $Gr_{\min}$ is a strong function of $k$ in the neighbourhood of $k = 0$ then the effects of any sidewalls could be important. The effects of a non-zero critical wave number and the importance of sidewalls are examined in the next section.

## 4. NUMERICAL SOLUTION

In this section, the full stability equations (26) are solved numerically with no assumptions made about the critical wave number. The method used is an adaptation of a method described by Patterson [16] which is an extension of a method described by Keller [17] for solving certain eigenvalue problems. The method is described briefly below.

Firstly, $\theta$ is eliminated from the marginal stability equations (26) leading to an equation for $\psi$

$$(\mathrm{D}^2 - k^2)^3 \psi = k^2 Gr_c \psi \mathrm{D}T^{(0)} \tag{36}$$

with the boundary conditions

$$\begin{aligned} &\psi = \mathrm{D}^2\psi = \mathrm{D}(\mathrm{D}^2 - k^2)\psi = 0 \quad \text{on} \quad z = 0 \\ &\psi = \mathrm{D}\psi = \mathrm{D}(\mathrm{D}^2 - k^2)\psi = 0 \quad \text{on} \quad z = -x. \end{aligned} \tag{37}$$

The above sixth order ordinary differential equation is translated into a system of six first order ordinary differential equations by introducing new variables $\psi^{(1)} = \mathrm{D}\psi$, $\psi^{(2)} = \mathrm{D}\psi^{(1)}, \ldots, \psi^{(5)} = \mathrm{D}\psi^{(4)}$. This leads to a system of equations that can be written in matrix form

$$\mathrm{D}\begin{bmatrix} \psi \\ \psi^{(1)} \\ \psi^{(2)} \\ \psi^{(3)} \\ \psi^{(4)} \\ \psi^{(5)} \end{bmatrix} = \begin{bmatrix} 0 & 1 & 0 & 0 & 0 & 0 \\ 0 & 0 & 1 & 0 & 0 & 0 \\ 0 & 0 & 0 & 1 & 0 & 0 \\ 0 & 0 & 0 & 0 & 1 & 0 \\ 0 & 0 & 0 & 0 & 0 & 1 \\ k^6 + k^2 Gr_c \mathrm{D}T^{(0)} & 0 & -3k^4 & 0 & 3k^2 & 0 \end{bmatrix} \begin{bmatrix} \psi \\ \psi^{(1)} \\ \psi^{(2)} \\ \psi^{(3)} \\ \psi^{(4)} \\ \psi^{(5)} \end{bmatrix} \tag{38}$$

with the boundary conditions

$$\begin{aligned} &\psi = \psi^{(2)} = \psi^{(5)} - 2k^2\psi^{(3)} + k^4\psi^{(1)} = 0 \ \text{on} \ z = 0 \\ &\psi = \psi^{(1)} = \psi^{(5)} - 2k^2\psi^{(3)} + k^4\psi^{(1)} = 0 \ \text{on} \ z = -x. \end{aligned} \tag{39}$$

The above formulation can be written in the more compact form

$$\begin{aligned} &\mathrm{D}\Psi - \mathbf{R}(z)\Psi = 0 \\ &\mathbf{A}\Psi|_{z=0} + \mathbf{B}\Psi|_{z=-x} = 0 \end{aligned} \tag{40}$$

where $\Psi$ is a six-row column vector of $\psi, \ldots, \psi^{(5)}$ and $\mathbf{R}(z)$ the $6 \times 6$ matrix of equation (38).

The system of equations (40) is now vertically discretized over $J$ grid points. Let $z_j = x(j\Delta z - 1)$,

$j = 0, \ldots, J$, where $\Delta z = 1/J$. Taking central differences about $j-1/2$ of equations (40) yields the system of algebraic equations

$$\frac{1}{\Delta z}(\Psi_j - \Psi_{j-1}) - \mathbf{R}((z_j + z_{j-1})/2)\tfrac{1}{2}(\Psi_j + \Psi_{j-1}) = 0, \qquad j = 1, \ldots, J \quad (41)$$

with

$$\mathbf{A}\Psi_0 + \mathbf{B}\Psi_J = 0. \quad (42)$$

The system of equations (41) and (42) can be written as

$$\begin{bmatrix} \mathbf{A} & 0 & 0 & \cdots & 0 & \mathbf{B} \\ \mathbf{E}_1 & \mathbf{D}_1 & 0 & \cdots & 0 & 0 \\ 0 & \mathbf{E}_2 & \mathbf{D}_2 & \cdots & 0 & 0 \\ \vdots & \vdots & \vdots & \ddots & \vdots & \vdots \\ 0 & 0 & 0 & \cdots & \mathbf{D}_{J-1} & 0 \\ 0 & 0 & 0 & \cdots & \mathbf{E}_J & \mathbf{D}_J \end{bmatrix} \begin{bmatrix} \Psi_0 \\ \Psi_2 \\ \Psi_3 \\ \vdots \\ \Psi_{J-1} \\ \Psi_J \end{bmatrix} = \mathbf{0} \quad (43)$$

where $\mathbf{E}_j$ and $\mathbf{D}_J$ are $6 \times 6$ matrices and are given by

$$\mathbf{E}_j = -\frac{1}{\Delta z}\mathbf{I} - \tfrac{1}{2}\mathbf{R}((z_j + z_{j-1})/2)$$

$$\mathbf{D}_j = \frac{1}{\Delta z}\mathbf{I} - \tfrac{1}{2}\mathbf{R}((z_j + z_{j-1})/2) \quad (44)$$

where $\mathbf{I}$ is the $6 \times 6$ identity matrix. Equation (43) can alternatively be written simply as $\mathbf{K}U = 0$ where $\mathbf{K}$ is a $6(J+1) \times 6(J+1)$ matrix and $U$ is a column vector with $6(J+1)$ elements. The equation $\mathbf{K}U = 0$ represents a system of $6(J+1)$ linear homogeneous equations in $6(J+1)$ unknowns. Since the system is homogeneous, the system will only have a non-trivial solution if $\det(\mathbf{K}) = 0$. The only variables of the problem are $Gr$ and $k$. This, then, forms the basis of the numerical method; finding the smallest positive $Gr$ that leads to the matrix $\mathbf{K}$ being singular.

The matrix $\mathbf{K}$ is $6(J+1) \times 6(J+1)$ and so calculating $\det(\mathbf{K})$ is computationally expensive for large values of $J$. The number of operations to calculate the determinant of a general $6(J+1) \times 6(J+1)$ matrix is $O((J+1)^2)$. However, by carrying out a little more manipulation, the problem can be further reduced, greatly speeding up the numerical solution.

Let $\mathbf{D} = \mathrm{diag}(\mathbf{I}, \mathbf{D}_1, \ldots, \mathbf{D}_J)$ then $\mathbf{D}^{-1} = \mathrm{diag}(\mathbf{I}, \mathbf{D}_1^{-1}, \ldots, \mathbf{D}_J^{-1})$. Premultiplying $\mathbf{K}$ by $\mathbf{D}^{-1}$ yields

$$\mathbf{D}^{-1}\mathbf{K} = \begin{bmatrix} \mathbf{A} & 0 & \cdots & 0 & \mathbf{B} \\ -\mathbf{P}_1 & \mathbf{I} & \cdots & 0 & 0 \\ \vdots & \vdots & \ddots & \vdots & \vdots \\ 0 & 0 & \cdots & \mathbf{I} & 0 \\ 0 & 0 & \cdots & -\mathbf{P}_J & \mathbf{I} \end{bmatrix} \quad (45)$$

where $\mathbf{P}_j = -\mathbf{D}_j^{-1}\mathbf{E}_j$. Postmultiplying the matrix $\mathbf{D}^{-1}\mathbf{K}$ by the matrix

$$\begin{bmatrix} \mathbf{I} & 0 & & & \\ 0 & \mathbf{I} & & & \\ & & \ddots & & \\ & & & \mathbf{I} & 0 \\ & & & \mathbf{P}_J & \mathbf{I} \end{bmatrix}$$

yields the result

$$\begin{bmatrix} \mathbf{A} & 0 & \cdots & 0 & \mathbf{B}\mathbf{P}_J & \mathbf{B} \\ -\mathbf{P}_1 & \mathbf{I} & \cdots & 0 & 0 & 0 \\ 0 & -\mathbf{P}_2 & \cdots & 0 & 0 & 0 \\ \vdots & \vdots & \ddots & \vdots & \vdots & \vdots \\ 0 & 0 & \cdots & \mathbf{P}_{J-1} & \mathbf{I} & 0 \\ 0 & 0 & \cdots & 0 & 0 & \mathbf{I} \end{bmatrix}. \quad (46)$$

Hence, defining $\pi_J = \mathbf{P}_J$ and $\pi_j = \pi_{j+1}\mathbf{P}_j$, $j = J-1, \ldots, 1$, the matrix $\mathbf{D}^{-1}\mathbf{K}$ can be diagonalized to the form

$$\mathbf{K}^* = \begin{bmatrix} \mathbf{A} + \mathbf{B}\pi_1 & \mathbf{B}\pi_2 & \cdots & \mathbf{B}\pi_J & \mathbf{B} \\ 0 & \mathbf{I} & \cdots & 0 & 0 \\ \vdots & \vdots & \ddots & \vdots & \vdots \\ 0 & 0 & \cdots & \mathbf{I} & 0 \\ 0 & 0 & \cdots & 0 & \mathbf{I} \end{bmatrix}. \quad (47)$$

Hence, $\det(\mathbf{K}) = 0 \Leftrightarrow \det(\mathbf{K}^*) = 0 \Leftrightarrow \det(\mathbf{A} + \mathbf{B}\pi_1) = 0$ where $\mathbf{A} + \mathbf{B}\pi_1$ is a $6 \times 6$ matrix. Calculating $\mathbf{A} + \mathbf{B}\pi_1$ takes $O(J+1)$ operations, considerably shortening the time it takes to test each value of $Gr$.

The aim of the algorithm, then, is to minimize over $k$ the smallest positive eigenvalue $Gr_{\min}$ for particular values of $x$ and $t$. This involves first fixing $k$ and then calculating the smallest eigenvalue $Gr_{\min}$ for that $k$. A Golden Section minimization procedure [18] is used to perform the minimization. This minimum and the associated $k$ at which it occurs are the critical values for the given $x$ and $t$.

All the calculations in this paper used 50 grid points. Increasing the number of grid points beyond 50 had no discernible effect on the results.

## 5. RESULTS AND DISCUSSION

Figure 5 shows a graph of $Gr_c$ calculated both numerically and analytically as a function of $x$ for various times. At $t = 0.05$, the two calculations have excellent agreement for $x < 1.1$ but for $x > 1.1$, the two curves diverge. Corresponding plots at different times display the same behaviour; excellent agreement for $x$ smaller than some critical value above which they diverge. For $x$ smaller than the critical value, the discussion at the end of Section 3 about the $k_c = 0$ solution is as relevant to the numerical calculation as it was for the analytical calculation.

The divergence of the analytical and numerical results in Fig. 5 can be attributed directly to a breakdown of the zero critical wave number assumption that is an essential part of the analysis of Section 3.

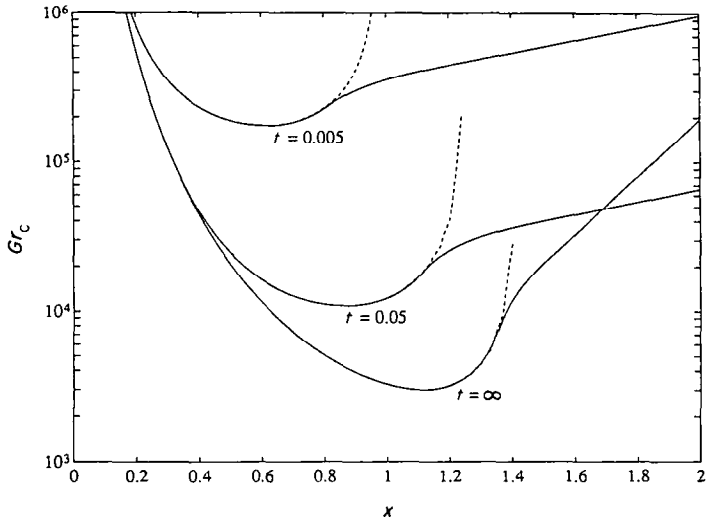


FIG. 5. Comparison between the numerically (solid) and analytically (dashed) (equation (35)) calculated critical Grashof number for various times. At $t = 0.05$, the analytical value $Gr_{c0}$ is negative for $x > 1.2$.

Figure 6 shows a plot of the numerically calculated critical wave number as a function of $x$ for various times. For $t = 0.05$ there is a clear bifurcation away from $k_c = 0$ at $x \approx 1.1$ just prior to the corresponding curves in Fig. 5 diverging. The reason for this jump has been discussed in Section 3 and is due to the unstable layer near $z = -x$ being isolated from the insulated upper boundary by a layer of stably stratified fluid. Note that in Fig. 5, the numerically calculated $Gr_c$ at $t = 0.0005$ and 0.05 are apparently exponential functions of $x$ for large $x$. This is consistent with the strength of the destabilizing boundary condition at $z = -x$ decaying like $e^{-x}$. Note also that for these times $k_c$ approaches a constant value as $x \to \infty$. This suggests that the thickness of the unstable layer near $z = -x$ is the same for all $x$. This is to be expected since the thickness of the unstable region is the same as the thickness of the conduction boundary layer near $z = -x$ since it is the boundary condition there that leads to the instability. A conduction boundary layer with thickness $\delta$ grows with time like $\delta \sim \sqrt{(\kappa t)}$ [19] which, importantly, is independent of the strength of the boundary heat flux and hence, in this case, independent of $x$ (as long as there are no other factors affecting its growth). This then explains the constant $k_c$ for large $x$. Also, the maximum unstable gradient in this region is $e^{-x}$ which, if applied over the conduction boundary layer, would lead to an

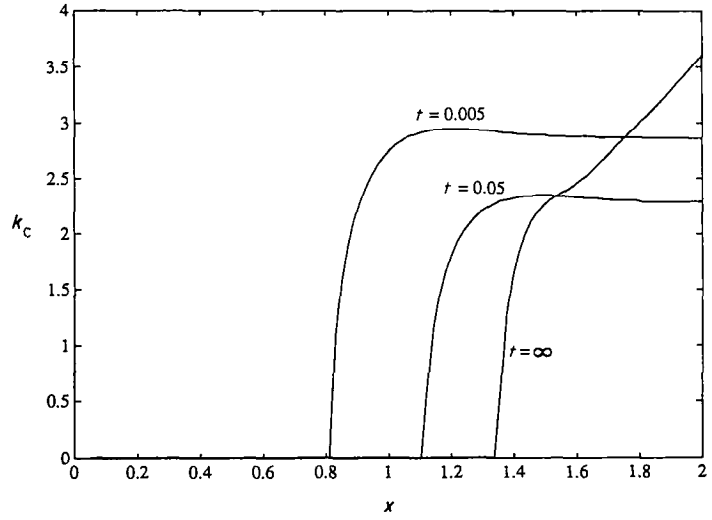


FIG. 6. Numerically calculated critical wave number as a function of $x$ for various times showing the bifurcation from $k_c = 0$. Note that for finite $t$, $k_c$ tends to a constant value as $x$ becomes large.

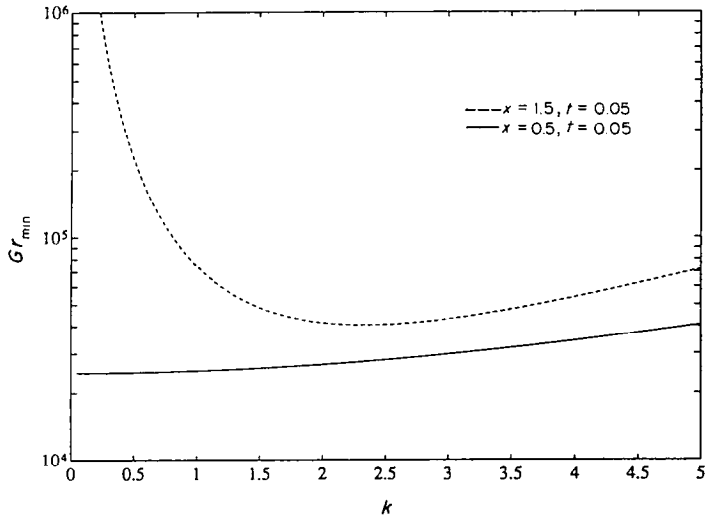


FIG. 7. Plots of the numerically calculated $Gr_c$ as a function of $k$ for $x = 0.5$ (solid line) and 1.5 (dashed line).

exponential growth of $Gr_c$ with $x$ which can be seen in Fig. 5. Finally, for finite $t$, $k_c$ tends to a constant value as $x \to \infty$ as can be seen in Fig. 6 and this value decreases as $t$ increases from 0.005 to 0.05 which is consistent with the instability being limited to the boundary layer.

The above argument does not apply as $t \to \infty$ since in this case, there is no boundary layer and the temperature profile is fully developed. Figure 5 shows that at $t = \infty$, $Gr_c$ still grows exponentially with $x$ as $x$ becomes large but at an increased rate. Figure 6 shows that for $t = \infty$, the critical wave number is apparently unbounded for large $x$ which is quite different to the large $x$ behaviour of the finite time case. The large time behaviour of $\partial T^{(0)}/\partial z$ is given by

$$\frac{\partial T^{(0)}}{\partial z} \to -e^z + \frac{1}{x}(z+x) \quad \text{as} \quad t \to \infty. \tag{48}$$

There are two competing heating mechanisms here; internal heating which is stabilizing and the boundary heating which is destabilizing. These two mechanisms are in balance within the water column when $T_z^{(0)} = 0$. If $z = -x+\xi$ then $T_z^{(0)} = 0$ if $\xi$ satisfies $x e^{-x} = \xi e^{-\xi}$. There are two roots to this equation, one of which is clearly $\xi = x$ which corresponds to the insulated upper boundary condition. The other root cannot be expressed in a closed form but denoting this root by $\xi_0$ then $\xi_0 \to x e^{-x}$ as $x \to \infty$. This shows that the point within the water column where the vertical temperature gradient vanishes moves closer to the lower

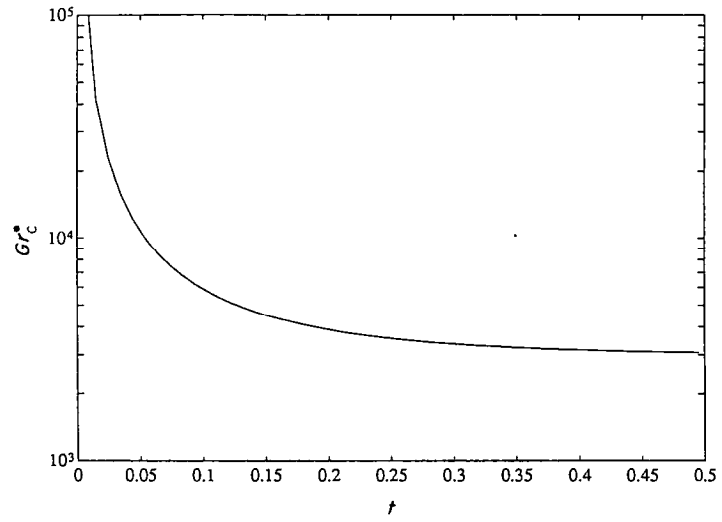


FIG. 8. The lower bound $Gr_c^*$ as a function of time as calculated in this paper.

boundary as $x$ becomes large. Thus, the thickness of the unstable region decreases with increasing $x$. This explains the large $x$ behaviour of the $t = \infty$ curves in Figs. 5 and 6. In Fig. 6, the wave number of the least stable mode scales with the inverse of the depth of the unstable layer and hence increases without limit as $x$ becomes large. In Fig. 5, two effects combine to give rise to a rapid increase in $Gr_c$ as $x$ increases. The first is the vanishing thickness of the unstable layer and the second is the decreasing magnitude of the unstable gradient across that layer. The former effect is absent in the finite time regime and thus the $t = \infty$ curve in Fig. 5 rises more rapidly for large $x$ than the finite $t$ curves.

In view of the fact that the critical wave number is a function of $x$, the question of wave number selection needs to be addressed. This is a complicated question and the results of this paper cannot provide a clear answer. Figure 7 shows a plot of $Gr_{min}$ (the smallest positive $Gr$ for secondary motion at each $k$) as a function of $k$ at two different values of $x$ at $t = 0.05$. At $x = 0.5$, the critical wave number is $k_c = 0$ while at $x = 1.5$, $k_c \approx 2.3$. This figure paints a rather confusing picture of how the secondary motion will develop. Note that for $x = 1.5$, $Gr_{min} \to \infty$ as $k \to 0$, that is, the temperature structure is unconditionally stable to zero wave number perturbations. This is consistent with the analytical solution $Gr_{c0}$ which is negative at $x = 1.5$. Graphs of $Gr_{min}$ for other values of $x$ above $x \approx 1.1$ show a similar behaviour. Thus, even if there is a region near the tip which is unstable with $k_c = 0$, away from the tip no such instability can occur. Alternatively, if there is an instability away from the tip with $k_c \neq 0$ then it is certainly possible to have secondary motion with $k_c \neq 0$ near the tip since the temperature profile there will be unstable to non-zero wave number disturbances if $Gr$ is sufficiently large. However, Chapman and Proctor [15], have shown that for a linear temperature profile and fixed flux boundary conditions such secondary flows will be unstable to smaller wave number disturbances though it is not clear that their results can be generalized to include the current case. Hence, one cannot conclude from the results of this paper what the nature of the secondary motion will be. This would require a full 3-D analysis with the possible inclusion of non-linear effects which is well beyond the scope of this paper.

## 6. CONCLUDING REMARKS

The aim of this paper was to determine a critical Grashof number $Gr_c$ below which one would expect the $O(A^2)$ solution of ref. [1] to be stable. This lower bound $Gr_c^*$ is plotted in Fig. 8 which shows $Gr_c^*$ as a function of time. At a particular time, for values of $Gr$ less than the corresponding $Gr_c^*$, the flow is stable for all values of $x$. For larger values of $Gr$, the flow is unstable in some region centred away from the tip.

Geophysical values of $Gr$ [3] range from $\sim 10^5$ for typical turbulent values of the diffusivity up to $\sim 10^{13}$ for molecular values. According to Fig. 8, both these values will be above the critical value after 12 h (which corresponds to $t \approx 0.025$ and 10 for molecular and turbulent diffusivities, respectively) which suggests that secondary motion will occur in real sidearms during the day. The secondary motion associated with the instability will be restricted to a small region near the shore since $Gr_c$ increases exponentially with distance from the tip. If the secondary motion has a long wavelength then it would be indistinguishable from the motion that would already exist because of the transverse topography. Alternatively, if the secondary motion has a short wavelength then it will consist of rising plumes of warm water emanating from the bottom boundary.

*Acknowledgements*—This work was carried out while the first author was a recipient of an Australian Postgraduate Research Award and a Centre for Water Research Scholarship. Both authors are grateful for the useful comments made by John Taylor and Andrew Barry on an earlier draft of this paper.

## REFERENCES

1. D. E. Farrow and J. C. Patterson, The daytime circulation pattern in a reservoir sidearm, Environmental Dynamics Reference ED-547-DF (1991).
2. A. Rabl and C. Nielson, Solar ponds for space heating, *Solar Energy* **17**, 1–12 (1975).
3. S. G. Monismith, J. Imberger and M. L. Morison, Convective motions in the sidearm of a small reservoir, *Limnol. Oceanogr.* **35**, 1676–1702 (1990).
4. J. R. Lloyd and E. M. Sparrow, On the stability of natural convection flow on inclined plates, *J. Fluid Mech.* **42**, 465–470 (1970).
5. E. M. Sparrow and R. B. Husar, Longitudinal vortices in natural convection flow on inclined surfaces, *J. Fluid Mech.* **37**, 251–255 (1969).
6. T. S. Chen and K. L. Tzuoo, Vortex instability of free convection over horizontal and inclined surfaces, *J. Heat Transfer* **104**, 637–643 (1982).
7. J. E. Hart, Stability of the flow in a differentially heated inclined box, *J. Fluid Mech.* **47**, 547–576 (1971).
8. J. E. Hart, Transition to a wavey vortex régime in convective flow between inclined plates, *J. Fluid Mech.* **48**, 265–271 (1971).
9. J. N. Shadid and R. J. Goldstein, Visualization of longitudinal convection roll instabilities in an inclined enclosure heated from below, *J. Fluid Mech.* **215**, 61–84 (1990).
10. P. C. Matthews, A model for the onset of penetrative convection, *J. Fluid Mech.* **188**, 571–583 (1988).
11. A. J. Roberts, An analysis of near-marginal, mildly penetrative convection with heat flux prescribed on the boundaries, *J. Fluid Mech.* **158**, 71–93 (1985).
12. T. D. Foster, Stability of a homogeneous fluid cooled uniformly from above, *Physics Fluids* **8**, 1249–1257 (1965).
13. J. L. Robinson, A note on the stability of an infinite fluid heated from below, *J. Fluid Mech.* **29**, 461–464 (1967).
14. P. M. Gresho and R. L. Sani, The stability of a fluid layer subjected to a step change in temperature: transient vs. frozen time analysis, *Int. J. Heat Mass Transfer* **14**, 207–221 (1971).
15. C. J. Chapman and M. R. E. Proctor, Non-linear Rayleigh–Bénard convection between poorly conducting boundaries, *J. Fluid Mech.* **101**, 749–782 (1980).

16. J. C. Patterson, Some elastic instability and associated problems with physiological applications. Ph.D. Thesis, Queensland (1974).
17. H. B. Keller, *Numerical Methods for Two-point Boundary-value Problems*. Blaisdell, London (1968).
18. W. H. Press, B. P. Flannery, S. A. Teukolsky and W. T. Vetterling, *Numerical Recipes, The Art of Scientific Computing*. Cambridge University Press, Cambridge (1986).
19. J. C. Patterson and J. Imberger, Unsteady natural convection in a rectangular cavity, *J. Fluid Mech.* **100,** 65-86 (1980).